Decoding the hidden variabilities in mPFC descending pathways across emotional states

Chien-Hsien Lai[1#], Gyeongah Park[2 #], Pan Xu[1,7#], Xiaoqian Sun[3], Qian Ge[2], Zhen Jin[2], Sarah Betts[1], Xiaojie Liu[4], Qingsong Liu[4], Rahul Simha[3], Chen Zeng[5], Hui Lu[1 *], Jianyang Du[2,6 *]

[1]Department of Pharmacology and Physiology, School of Medicine and Health Sciences, The George Washington University, Washington, DC 20037, USA

[2]Department of Anatomy and Neurobiology, University of Tennessee Health Science Center, Memphis, TN 38163, USA.

[3]Department of Computer Science, School of Engineering and Applied Science, The George Washington University, Washington, DC 20037, USA

[4]Department of Pharmacology and Toxicology, Medical College of Wisconsin, Milwaukee, WI 53226, USA

[5]Department of Physics, Columbia College of Art and Sciences, The George Washington University, Washington, DC 20037, USA

[6]Neuroscience Institute, University of Tennessee Health Science Center, Memphis, TN, United States.

[7]Present address: Medical Science and Technology Innovation Center, Shandong First Medical University & Shandong Academy of Medical Sciences, Jinan, Shandong 250000, China

*Corresponding author: Jianyang Du, Ph.D., jdu15@uthsc.edu; Hui Lu, Ph.D., huilu@email.gwu.edu.

# These authors contributed equally to this work.

ABSTRACT

Effective emotional regulation, crucial for adaptive behavior, is mediated by the medial prefrontal cortex (mPFC) via connections to the basolateral amygdala (BLA) and nucleus accumbens (NAc), traditionally considered functionally similar in modulating reward and aversion responses. However, how the mPFC balances these descending pathways to control behavioral outcomes remains unclear. We found that while overall firing patterns appeared consistent across emotional states, deeper analysis revealed distinct variabilities. Specifically, mPFC→BLA neurons, especially "center-ON" neurons, exhibited heightened activity during anxiety-related behaviors, highlighting their role in anxiety encoding. Conversely, mPFC→NAc neurons were more active during exploratory behaviors, implicating them in processing positive emotional states. Notably, mPFC→NAc neurons showed significant pattern decorrelation during social interactions, suggesting a pivotal role in encoding social preference. Additionally, chronic emotional states affected these pathways differently: positive states enhanced mPFC→NAc activity, while negative states boosted mPFC→BLA activity. These findings challenge the assumed functional similarity and highlight distinct contributions to emotional regulation, suggesting new avenues for therapeutic interventions.

INTRODUCTION

Recent advancements in neuroscience have significantly advanced our understanding of the complex roles played by the medial prefrontal cortex (mPFC) pathways to the basolateral amygdala (BLA) and nucleus accumbens (NAc). These pathways are pivotal in emotional and motivational processing, mediating behaviors that involve assessing conflicts between reward and aversion, thus enabling the brain to adaptively respond to diverse environmental stimuli (1, 2).

Both the mPFC→BLA and mPFC→NAc pathways are integral in regulating emotional responses and influencing decision-making under conditions of potential reward and threat (3). This regulation is crucial in contexts where reward-seeking behaviors are curtailed in the presence of aversive stimuli, highlighting a shared role in managing the delicate balance between risk and reward during emotional and motivational conflicts.

The mPFC-amygdala interconnection functions as an integrative nucleus for evaluating reward-aversion conflicts. Key studies, such as by Ishikawa et al. have shown that IL projections to the BLA must be active to suppress reward-seeking when paired with electric shock punishment (4). This modulation may be related to the BLA's influence on the NAc shell, as explored by Piantadosi et al. (5). Additionally, Diehl et al. have demonstrated that the PL-BLA-NAc shell circuit is involved in active avoidance, with direct projections from the PL to the NAc core inhibiting avoidance, while indirect projections via the amygdala facilitate it after a tone-shock association (6).

Furthermore, studies such as those by Warlow et al. and Martínez-Rivera et al. underline the plasticity of motivational valence and activation patterns during active avoidance, showing activation of both PL and IL projections to the NAc during the extinction of avoidance behaviors (7, 8). Kim et al. discovered that stimulating mPFC-NAc lateral shell neurons, activated by an aversive stimulus, can suppress reward-seeking behavior, emphasizing the mPFC-NAc pathway’s critical role in balancing pleasure and harm (9).

These findings confirm the fundamental similarities in how these pathways modulate emotional responses and also underscore significant differences in their mechanisms and behavioral impacts. Although substantial progress has been made, many questions about the neural mechanisms within these mPFC pathways remain unresolved. Traditional methods, such as pharmacological interventions, c-fos expression studies, circuit tracing, and optogenetics, have provided foundational insights but lack the precision needed to manipulate specific emotion-related neurons. These techniques often do not correspond to distinct cell types or function-specific subpopulations that could be selectively targeted. Consequently, the nuanced functional differences at the cellular and circuit levels between these pathways might remain hidden, limiting our understanding of their functions.

Utilizing in vivo imaging to investigate the network dynamics within the mPFC→BLA and mPFC→NAc pathways, we aim to explore both the similarities and differences in how these pathways process emotions. Specifically, we are interested in understanding how similar or distinct the neuronal activation patterns and network dynamics are between these two pathways during emotional processing tasks. This includes examining the temporal and spatial characteristics of neuronal population activity and how these patterns correlate with specific emotional behaviors. We notably utilized a social competition behavioral paradigm to induce emotional states in mice, which allowed us to examine synaptic changes within these pathways. Our research revealed distinct circuit dynamics and plasticity patterns in these two pathways that correlate directly with various emotional states in mice.

RESULTS

Differential activity pattern of neurons in the mPFC→NAc and mPFC→BLA neurons in response to anxiety and exploration-inducing stimuli

To distinguish the mPFC→BLA and mPFC→NAc neurons, we employed retrograde AAV viruses carrying genes encoding the calcium (Ca^{2+}) indicator GCaMP6m, delivering them to the BLA and NAc of adult female wildtype mice at the age of ~20 weeks, respectively **(Fig. 1A)**. This allowed for the infection of mPFC neurons projecting to either of these regions, leading to

GCaMP6 expression in the soma situated in the mPFC **(Fig. 1B)**. In vivo Ca^{2+} imaging was conducted on mPFC→BLA and mPFC→NAc neurons using a portable miniaturized microscope **(Fig. 1C)**. The activity of individual neurons was continuously monitored throughout the behavioral assays. We synchronized the Ca^{2+} imaging with the behavioral recordings, following the same neurons within each mouse across the different test sessions (see Methods).

We first performed the open field test (OFT), a widely employed behavioral assay in rodent research for assessing exploratory and anxiety-like behaviors **(Fig. 1D)**. This test leverages the inherent conflict rodents experience between their desire to explore new environments and their instinctive aversion to exposed spaces. We monitored and recorded the mouse's movements and actions over a 10-minute period, specifically tracking time spent in the center versus the corner, wall-sniffing, and grooming. These behaviors observed during the open field test-spending time in corners, the center area, grooming, and sniffing walls **(Fig. 1E)** —offer valuable insights into their emotional states. Typically, mice in corners exhibit lower anxiety levels, suggesting a sense of security. Conversely, exposure to the center area may induce higher anxiety due to increased exposure and reduced safety compared to the arena's edges or corners. Grooming behaviors can signal stress relief or comfort, while wall-sniffing reflects sensory exploration and vigilance, possibly indicating curiosity, cautious exploration, or heightened alertness (10, 11). Our findings demonstrate that mice consistently spend significant time in corners during the 10-minute session. Additionally, they allocate around 10% of the time to the center area or grooming, and approximately 5% of the time to wall-sniffing **(Fig. 1F)**. The sniffing time is excluded from the corner-dwelling time if sniffing takes place in the corner area.

To determine whether the pattern of neuronal activities in the mPFC→BLA and mPFC→NAc pathways differs in response to different emotional statuses, we first estimated the Ca^{2+} transient rate. During our observation of mPFC→BLA and mPFC→NAc neuron activity **(Fig. 1G)** during the open field test, we determined that the collective averaged Ca^{2+} transient rate of the neurons in these two pathways did not exhibit discernible differences while the mice were situated in the center, corner, or during sniffing or grooming **(Fig. 1H)**. To delve deeper, we conducted a Principal Component Analysis (PCA) to assess the population activity pattern linked to various behaviors, encompassing center or corner dwelling, grooming, and sniffing. The PCA plots in

Fig. 1I reveal how neuronal activities associated with various behaviors differ between these pathways, with each point representing recorded neuronal activity during specific behaviors projected onto the first two principal components (PC1 and PC2). These components capture the most significant variances within the dataset. These two plots display distinct clustering of activity patterns with clear separations among the different behaviors, particularly between center and corner behaviors, as well as sniffing and grooming. We quantified the distances from the Corner behavior for different behavioral states across two pathways **(Fig. 1J)**. The significant differences in behaviors such as Center, Sniffing, and Grooming suggest distinct neural representations within these pathways. Notably, while both pathways exhibit similar patterns for Corner behavior, suggesting comparable neural processing **(Fig. 1I)**, the Center and Grooming behaviors show markedly greater distances from Corner behavior in the mPFC→BLA pathway, indicating more differentiated neural encoding. This pronounced differentiation, especially notable in the Grooming behavior within the mPFC→BLA pathway, suggests a crucial role in distinguishing between states of anxiety-related and non-anxiety behaviors **(Fig. 1I and J)**. Furthermore, the mPFC→NAc pathway demonstrates a more dominant role in distinguishing exploratory behavior (Sniffing) from Corner behavior, highlighting its unique contributions in processing exploration versus anxiety **(Fig. 1I and J)**. This analysis underlines the distinct roles of the mPFC→BLA and mPFC→NAc pathways in behavioral differentiation, with the mPFC→BLA pathway showing stronger distinctions in anxiety-related and non-anxiety behaviors, and the mPFC→NAc pathway more specifically delineating exploratory behaviors from those driven by anxiety.

The above differentiation in population activity was not revealed by averaging the transient rate. When considering averaging transient rate across a population can potentially mask characteristics unique to neurons that represent the emotional states of mice associated with these behaviors, we thus narrowed our focus to neurons that exhibited increased activity during heightened anxiety moments, such as entering the center zone. Termed "center-ON" neurons, these neurons displayed substantially increased spikes around the mouse's entry into the center zone, suggesting their response to emotional shifts from low (prior to entry) to high (post-entry into the anxiety-inducing center zone) states **(Fig. 2A)**. This increase in activity of the center-ON neurons in the mPFC→BLA pathway was not observed when the mice entered corner zones or

engaged in sniffing or grooming **(Fig. 2B)**. Upon comparing the percentage of center-ON neurons in the two pathways, we observed a higher prevalence of center-ON neurons in the mPFC→BLA group compared to the mPFC→NAc group **(Fig. 2C)**. This finding supports the earlier observation that there is more pronounced coding of anxiety states by neurons in the mPFC→BLA pathway compared to those in the mPFC→NAc pathway. When we projected the activity patterns of these center-ON neurons onto the spatial distribution of the open field arena **(Fig. 2D)**, both sets of center-ON neurons displayed heightened activity in the center zone. However, the center-ON neurons in the mPFC→NAc population exhibited increased activity during sniffing as well, which was not observed in the mPFC→BLA population **(Fig. 2E)**. This finding implies that these two sets of center-ON neurons serve distinct roles in encoding the emotional states of the mice. Specifically, the mPFC→NAc neurons appear to be more involved in positive emotional states associated with exploration, while the mPFC→BLA neurons are more associated with negative emotional states related to anxiety. To reinforce this notion, we conducted the PCA exclusively on the center-ON neuron populations **(Fig. 2F)**. Intriguingly, PCA scatter plots reveal behavioral clustering and spatial separations, demonstrating different behaviors influence neuronal engagement differently in these two pathways. Again, we quantified the distances of neuronal activity patterns associated with Center, Sniffing, and Grooming from Corner behavior in both pathways **(Fig. 2G)**. The result showed significant differences in encoding emotional states between the center-ON ensembles of the two pathways. Similar to **Fig. 1J**, the greater distance of Center behavior from Corner behavior in the mPFC→BLA pathway suggested that the mPFC→BLA pathway may play a critical role in modulating stress and anxiety responses, highlighting its potential as a target for interventions in anxiety disorders. Conversely, the mPFC→NAc pathway appears more involved with general exploratory behaviors and less specialized in handling anxiety-specific processing **(Fig. 2F and G)**. The observation of center-ON neurons could reveal more dominant differentiation in the function of the two pathways, mPFC→BLA and mPFC→NAc.

Distinct activation of center-ON Neurons in response to anxiety-inducing stimuli

To further validate our previous findings, we conducted the Elevated Plus Maze (EPM) test with the same mice one day following the OFT, as shown in **Fig. 3A**. The EPM test assesses anxiety

by noting whether mice explore the exposed and elevated open arms (indicative of higher anxiety) or prefer the sheltered, enclosed arms (indicative of lower anxiety). Our observations revealed that mice predominantly stayed in the closed arms, particularly favoring one closed arm (preferred closed arm, closed-P) over the other (non-preferred closed arm, closed-NP), suggesting a strong preference for a safer environment, despite both closed arms being designed to offer security **(Fig. 3B)**. Neuronal activity in the mPFC→BLA and mPFC→NAc pathways was recorded during the EPM test. The neurons exhibited increased transient rates in the open arms, indicative of an anxiety response, though no significant differences were observed in the overall activity patterns between these pathways **(Fig. 3C)**. This is consistent with earlier results from the OFT **(Fig. 1H)**. Subsequent analyses focused on "center-ON" neurons previously identified during the OFT, examining their responses across different states in the EPM **(Fig. 3D and E)**. Notably, center-ON neurons in the mPFC→BLA pathway demonstrated significantly heightened activity in the open arms compared to the closed arms, particularly when mice entered the open arms **(Fig. 3F)**. The Ca^{2+} transient rates for these neurons were markedly higher than those in the mPFC→NAc pathway, especially when mice were in the less familiar open-NP arm, suggesting that the unfamiliarity of this arm amplifies anxiety, and the mPFC→BLA pathway is particularly sensitive to this increase **(Fig. 3G)**. These findings corroborate our initial observations from the OFT, emphasizing the mPFC→BLA neurons' critical role in modulating responses to anxiety-driven emotional states in mice. The pronounced activity differences in these specific neurons highlight their potential role in more acutely perceiving and processing anxiety-inducing stimuli. These findings suggest that center-ON neurons in the mPFC→BLA pathway may have a more substantial role in responding to and possibly regulating anxiety states compared to the mPFC→NAc pathway.

The mPFC→NAc neurons, as opposed to mPFC→BLA neurons, encode emotional information associated with social preference.

The social behavior can effectively reflect various emotional states in individuals (12) and is encoded by the mPFC neuron ensembles with distinct activity patterns (13). We thus investigated whether distinct activity patterns are exhibited by mPFC→BLA and mPFC→NAc neurons, correlating with different social states. The social test was conducted using a three-chamber

apparatus **(Fig. 4A)**. The two end chambers were equipped with either another mouse or an object. The subject mouse underwent a 10-minute acclimation phase in the central 45 cm chamber, with the 10 cm end compartments empty. Subsequently, three ten-minute testing sessions (S1, S2, and S3) were conducted, each involving different stimuli in the end chambers to assess interaction. Utilizing automated tracking software, the time spent within the "sniffing zone" was measured. Notably, the mice exhibited a preference for interacting with fellow mice over objects in S1 and S2. In S2, this preference gap narrowed due to the relocation of objects. Remarkably, during S3, wherein the choice was between two mice, the mice displayed a greater inclination to explore the new mouse **(Fig. 4B)**. These findings collectively signify a normal level of sociability as observed in the three-chamber test.

To explore the neuronal activity associated with distinct social states, we closely monitored the excitatory mPFC→BLA and mPFC→NAc neurons within the prelimbic region of the mPFC. Surprisingly, both the mPFC→BLA and mPFC→NAc neurons exhibited little discernible difference in their Ca^{2+} transient rate while the mice interacted with the social stimulus (mouse 1, M1) and the nonsocial stimulus (object, O) **(Fig. 4C and D)**. Likewise, no significant variation emerged during session 3. Given that interactions with social and nonsocial stimuli are known to induce differing emotional states, as reflected in social preference, our findings suggested that the neural encoding of these distinct emotional states was not reliant on the overall firing rate of the mPFC→BLA and mPFC→NAc neurons.

Next, we analyzed the ability of these two groups of neurons to convey information through coactivity patterns (14). Functional correlations (coactivity) within the circuit can be identified using Pearson correlation coefficients, and pattern decorrelation serves to clarify overlapping activity patterns. This mechanism is akin to how the olfactory bulb distinguishes closely related odorants based on minor structural variations (7, 15, 16). In a previous study, we demonstrated that pattern decorrelation of mPFC excitatory circuit neuronal activities is indispensable for social preference (17). This led us to contemplate whether differences existed between the mPFC→BLA and mPFC→NAc neurons. We thus calculated the pairwise Pearson correlation coefficients of neuronal activities specifically during the interaction with the social or object stimulus **(Fig. 4E and F)**. The pairwise correlation coefficients for different stimuli across the

recorded mPFC→BLA and mPFC→NAc neurons from all mice exhibited a distribution around zero, albeit with varying widths. Intriguingly, we observed a significant pattern decorrelation only within the mPFC→NAc neurons, evident by the full-width at half maximum (FWHM) of the correlation distribution being lower for the more attractive stimuli in each session (**Fig. 4F**). In contrast, such decorrelation was not observed in the mPFC→BLA neurons (**Fig. 4 G** and **H**), indicating that mPFC→NAc neurons play a more prominent role in encoding social preference and emotional states through distinct coactivity patterns. These results suggest that the mPFC→NAc pathway is more actively involved in processing and guiding social behavior, while mPFC→BLA neurons may play a lesser role in differentiating between social and nonsocial stimuli based on their coactivity.

We next explored the distinct activity patterns of mPFC→BLA and mPFC→NAc neurons during social (M1) and nonsocial (object, O) interactions by comparing all recorded neurons and the subset of center-ON neurons previously identified **(Fig. 5)**. The PCA analysis for all recorded neurons in both pathways showed that the mPFC→BLA neurons exhibit greater separation between social (M1) and nonsocial (O) stimuli than the mPFC→NAc neurons **(Fig. 5A)**. This indicates that mPFC→BLA neurons display a more distinct encoding of social and nonsocial interactions. We quantified the distance between the neuronal activity clusters for social and nonsocial stimuli, showing a significantly greater separation in the mPFC→BLA pathway compared to the mPFC→NAc pathway, supporting the notion that mPFC→BLA neurons are more attuned to distinguishing between these stimuli **(Fig. 5B)**. We then focused specifically on center-ON neurons identified during the OFT. The PCA plots showed that the center-ON neurons in the mPFC→NAc pathway exhibited more distinct separation between social and nonsocial stimuli compared to the mPFC→BLA neurons which showed much less differentiation **(Fig. 5C)**. We further quantified the distances between social and nonsocial stimuli for center-ON neurons, with mPFC→NAc neurons showing significantly greater separation compared to mPFC→BLA neurons **(Fig. 5D)**. Overall, the result demonstrated that, while mPFC→BLA neurons show more general population-level encoding of social versus nonsocial stimuli, the mPFC→NAc pathway is more specialized in differentiating these stimuli within behaviorally relevant neuronal subsets (center-ON neurons). This highlights distinct roles for these pathways in encoding and processing social and nonsocial information, with mPFC→BLA neurons

contributing to broader environmental differentiation and mPFC→NAc neurons being more involved in social preference encoding.

The mPFC→NAc and the mPFC→BLA neurons were manipulated distinctly by chronic emotional states.

Demonstrating the mPFC→NAc and mPFC→BLA neurons as encoding acute positive (exploration) and negative (anxiety) emotions, respectively, led us to question whether these pathways could also be influenced by naturally induced emotional states. Competitions, such as winning or losing, are effective natural means to induce opposite emotions. The social dominance tube test, commonly used to evaluate social hierarchy and aggression in rodents, serves as an ideal method for natural emotion induction. It involves placing two mice in a clear narrow tube to observe their interactions as they navigate toward opposite ends (18-22). Repeated daily over a week, this procedure often results in mice adopting consistent winner or loser roles, potentially leading to sustained positive or negative emotional states.

To verify if the tube test genuinely altered emotional states, littermate mice underwent an open field test both before and after the tube test **(Fig. 6A)**. Initially, there was no difference in the travel distance or time spent in the center of the open field arena between winner and loser mice **(Fig. 6B)**. Post-tube test, travel distances remained unchanged, suggesting that mobility was not affected by induced emotions. However, loser mice spent significantly less time in the center, indicating heightened anxiety and successful negative emotion induction. In contrast, winners' time in the center remained unchanged, implying their anxiety levels remained normal **(Fig. 6C and D)**. Furthermore, to determine if the tube test could evoke positive emotions in winner mice, their sociability was assessed before and after the test because positive emotion (such as the pleasure from winning) would enhance sociability **(Fig. 6E)**. Initially, both the winner and loser mice showed a standard preference for interacting with a live mouse over an inanimate object, and a new mouse over a familiar one **(Fig. 6F)**. After the tube test, winners displayed a higher sociability index towards social mice and a tendency for greater interest in new mice. In contrast, losers almost entirely lost their social preference, underscoring the induction of negative emotions **(Fig. 6G and H)**. These findings confirm that the repeated competitions in the tube test

successfully induced distinct positive and negative emotions in the winner and loser mice, respectively.

Next, we compared the synaptic strength in the mPFC→NAc and mPFC→BLA circuits following emotion induction via the repeated tube test. To activate these circuits, we used AAV-mediated expression of channelrhodopsin-2 (ChR2) for selective stimulation of prelimbic (PL) neurons in the NAc and BLA using blue light. ChR2-EYFP expression was verified in the PL, with terminal expression in the NAc and BLA **(Fig. 7A and B)**. Following the establishment of stable social rankings through the tube test **(Fig. 7C)**, we recorded from brain slices containing the NAc or BLA. Blue light application confirmed ChR2 activation, triggering inward currents and action potentials in both winner and loser mice **(Fig. 7D and H)**. In the mPFC→NAc pathway, blue light stimulation evoked larger excitatory postsynaptic currents (EPSCs) in winner mice compared to losers **(Fig. 7E)**, despite similar paired-pulse ratios (PPRs) in both groups **(Fig. 7F and G)**. This suggests stronger synaptic transmission in winners' mPFC→NAc circuits. Conversely, in the mPFC→BLA pathway, loser mice exhibited larger EPSCs and significantly higher PPRs than winners **(Fig. 7I-K)**, indicating stronger synaptic transmission in losers' mPFC→BLA circuits. Indeed, we found that the AMPA/NMDA receptor-mediated EPSC ratio was higher in winners' mPFC→NAc circuits and losers' mPFC→BLA circuits **(Fig. 7L and M)**. This result showed that winning and losing influence distinct neural pathways, with winners enhancing synaptic transmission in the mPFC→NAc circuit and losers in the mPFC→BLA circuit.

Importantly, we observed no significant differences in synaptic strength between winner and loser mice within the mPFC region. The correlation between the light intensity and the normalized amplitude of blue light-induced current showed no variance between the winner and loser groups during light stimulation and recordings in the PL region of the mPFC **(Fig. 8A-C)**. Furthermore, the induction of emotional states did not alter the excitability of mPFC neurons; this is evident from the consistent relationship between light stimulation frequency and the number of action potentials induced across mPFC neurons from both winner and loser mice **(Fig. 8D and E)**. Consequently, it appears that the induction of emotion specifically affects the descending pathway from the mPFC, rather than the neuronal activity within the mPFC itself.

Overall, our findings reveal that chronic positive emotions correlate with enhanced synaptic strength in the mPFC→NAc pathway, while chronic negative emotions are linked to increased synaptic strength in the mPFC→BLA pathway. These outcomes underscore the divergent modulation of mPFC inputs to the NAc and BLA by positive and negative emotional states, further illuminating the distinct roles of these circuits in encoding emotional states with opposite valence.

DISCUSSION

This study delves into the differential roles of the medial prefrontal cortex (mPFC) pathways to the basolateral amygdala (BLA) and the nucleus accumbens (NAc) in processing emotional and social stimuli. Through a combination of behavioral assays and neural recordings, we observed that while both pathways participate in emotion and social behavior coding, they exhibit distinct dynamics.

The mPFC→BLA pathway demonstrated a broader capacity to differentiate between a range of emotional states, particularly anxiety, suggesting a generalized role in emotional processing across various stimuli. In contrast, the mPFC→NAc pathway, especially its center-ON neurons, was more finely tuned to specific exploratory behavior or social interactions, suggesting their involvement in processing reward-related information and exploration behavior (23, 24). This differentiation is most evident in the context of anxiety, where the mPFC→BLA neurons show enhanced responsiveness, highlighting their pivotal role in anxiety management. This observation concurs with prior research highlighting the Amygdala's pivotal role in fear and anxiety processing (25, 26).

The contrasting patterns of neuronal activity observed between "center-ON" neurons and the entire neuronal population further underscore the functional diversity within the mPFC→BLA and mPFC→NAc pathways **(Fig. 1 and 2)**. The broader population of neurons does not exhibit the same selective sensitivity to emotional changes. Instead, their activity appears to be more generalized, without showing the same level of specificity as "center-ON" neurons. This suggests that while the overall activity of these pathways may play a role in modulating emotional states,

it is the specialized subset of "center-ON" neurons that provides the most nuanced and accurate representation of emotional shifts, particularly those related to anxiety. In essence, "center-ON" neurons act as a specialized subset that finely tunes the encoding of emotional states in response to specific triggers, such as entry into anxiety-inducing environments. This specialized encoding provides a more detailed and precise understanding of the mice's emotional responses to various situations. On the other hand, the broader neuronal population within these pathways contributes to the overall regulation of emotional responses, albeit in a less specialized manner. Together, these findings highlight the complexity of neural processing by demonstrating the coexistence of specialized and generalized encoding mechanisms within neural circuits. This complexity underscores the nuanced ways in which neural circuits process emotional cues, emphasizing the critical roles of distinct pathways in shaping the multifaceted landscape of emotional responses.

Based on the result on social behavior, a nuanced understanding of how different subsets of neurons within the mPFC pathways respond to social and nonsocial stimuli emerges: For the entire neuronal population: The mPFC→BLA pathway shows significantly greater differentiation between social and nonsocial stimuli compared to the mPFC→NAc pathway **(Fig. 5A and B)**. This suggests that, on a broad scale, the mPFC→BLA neurons are more adept at encoding differences between these stimuli types, potentially facilitating a generalized response to varied environmental contexts. This generalized role is important because anxiety can be triggered by a variety of stimuli, not strictly social or nonsocial, and may require a more holistic neural processing strategy that the mPFC→BLA neurons provide. For the center-ON neurons: Contrary to the broader neuronal population, when focusing on the center-ON subset, the mPFC→NAc pathway exhibits significantly greater differentiation between the stimuli than the mPFC→BLA pathway **(Fig. 5C and D)**. This indicates that within this specific subset of behaviorally relevant neurons, the mPFC→NAc pathway is finely tuned to discern between social and nonsocial stimuli, possibly playing a critical role in more nuanced or specific social behaviors. Therefore, the differing roles of the mPFC→BLA and mPFC→NAc pathways highlight a complex, layered approach to the neural encoding of social and nonsocial stimuli within the brain. While the mPFC→BLA neurons provide a broad, generalized framework for environmental differentiation, the center-ON neurons in the mPFC→NAc pathway specialize in sharply defining distinctions between social interactions and inanimate objects. This dual-layered

encoding system may allow for both flexible adaptation to general environmental changes and precise behavioral responses in socially nuanced situations.

Furthermore, our study has uncovered a fascinating dimension regarding the impact of chronic emotional states on the synaptic strength within these specific neuronal pathways. Notably, we observed that sustained positive emotional states were linked to a reinforcement of synaptic strength in the mPFC→NAc pathway **(Fig. 7E)**. This aligns well with the NAc's recognized function in processing rewards and promoting positive reinforcement (27, 28). In contrast, chronic negative emotional states correlated with heightened synaptic strength in the mPFC→BLA pathway **(Fig. 7I-K)**, further affirming the BLA's pivotal role in processing aversive stimuli and triggering fear responses (29, 30). Significantly, these findings highlight the potential influence of social status on the reward and emotional processing associated with the mPFC descending pathways. This insight offers a critical understanding of the neural circuit mechanisms that govern an animal's emotional state within real-world environments characterized by hierarchical dynamics. However, further research is warranted to delve into the molecular and cellular mechanisms underlying these effects and to ascertain if analogous effects manifest in other brain regions implicated in social status-dependent emotional states.

In summary, our study sheds light on the intricate interplay between distinct mPFC neuronal pathways and their modulation in response to various emotional states and environmental cues. The BLA-projecting neurons appear to play a pivotal role in encoding negative emotional states and responding to anxiety-inducing environments, while the NAc-projecting neurons contribute to positive emotional states and exploration. These results enhance our knowledge of the neural circuits involved in emotional processing and behavior, setting the stage for more in-depth studies into the intricate mechanisms of emotional regulation and their possible implications for neuropsychiatric disorders.

METHODS AND MATERIALS

Animal care and usage followed NIH Guidelines and received approval from the Institutional Animal Care and Use Committee of George Washington University and The University of

Tennessee Health Science Center Laboratory Animal Care Unit.

Experimental Animals

CaMKII-Cre mice with a pure C57BL/6 background were acquired from Jackson Lab (JAX#005359). For excitatory neuron imaging experiments, female CaMKII-Cre mice were bred by mating male CaMKII -Cre mice with female mice from the 129S1/SvlmJ strain (JAX#002448). These experimental CaMKII -Cre mice were used in accordance with the same procedural guidelines. Surgeries were performed on mice at approximately 4 months of age, adhering to the established experimental protocol. Animals were housed in groups of 4 to 5 per cage in a controlled environment with a temperature of 23 ± 1°C, humidity set at 50 ± 10%, and a 12-hour light-dark cycle. Standard mouse chow and water were provided ad libitum.

Virus injection and gradient-index (GRIN) lens implantation

In the context of imaging excitatory neurons, we employed the AAV1-EF1a-flex-GCaMP6m virus acquired from Baylor College of Medicine. Following established protocols (17), CaMKII -Cre mice were anesthetized and securely positioned within a Neurostar stereotaxic frame from Tübingen, Germany. Employing a high-speed rotary stereotaxic drill (Model 1474, AgnTho's AB, Lidingö, Sweden), we conducted a unilateral injection of the retrograde virus into either the left Nucleus Accumbens (NAc) region (anterior-posterior AP: +1.34 mm, medial-lateral ML: -1.1 mm, dorsal-ventral DV: 4.4mm) or Amygdala region (AP: -1.6 mm, M/L: -2.9 mm, DV: 4.5mm) using the Nanojector II system from Drummond Scientific. The injection comprised 300 nL of virus diluted with 300 nL of PBS, administered at a controlled rate of 30 nL/min. Post-injection, the needle was retained in place for an additional 5 minutes to optimize virus diffusion. Subsequent to viral injection, a precise 1.1 mm-diameter craniotomy was conducted at AP: +1.95 mm, M/L: -0.5 mm coordinates. These values were determined relative to bregma: +1.95 mm AP, -0.35 mm ML, -2.3~-2.5 DV, employing a high-resolution atlas. Following this, a 1-mm diameter GRIN lens (Inscopix, Palo Alto, CA) was progressively lowered into the left PL region (AP: +1.95 mm; ML: ± 0.35 mm; DV: -2.1~-2.3 mm) at a rate of 50 μm/min, situated 0.2 mm above the virus injection site, and then cemented in place using Metabond S380 (Parkell).

Subsequently, the mice were allowed to recover on a heating pad and were closely monitored over the ensuing 7 days, during which they received analgesic treatment.

Baseplate attachment

Around three to four weeks post-surgery, we assessed virus expression in the anesthetized mice using a miniaturized microscope from Inscopix, based in Palo Alto, CA. Once GCaMP+ neurons were clearly visible, we proceeded to attach the microscope with a baseplate onto the mouse's skull window. This setup was then gradually lowered to determine the optimal focus plane. Subsequently, the baseplate was securely affixed to the skull using dental cement and covered with a protective cap, while the microscope remained unattached. Ahead of the behavioral tests, the mice were familiarized with the test room environment, during which a dummy microscope was mounted and handled for approximately 5 to 7 days, with sessions lasting 30 to 40 minutes each day.

Selection of animals

Mice were chosen based on specific criteria: for the observation of Ca^{2+} signals in the mPFC, mice were excluded post-hoc if (1) the GRIN lens was positioned outside of the prelimbic cortex, (2) GCamp6 was not expressed within prelimbic areas, (3) significant virus expression was observed outside of the prelimbic region, and (4) the imaging plane was obstructed by blood or debris. In the identification of mPFC neural ensembles, mice exhibiting no center entry behavior were excluded, as the classification was grounded in the neural responses to transitions in location.

Determination of sample size

The sample sizes for behavioral experiments were established following the prevailing standards in behavioral neuroscience research for mice. This approach considers the minimum number of mice needed to detect statistical significance, with an α level of 0.05, and a statistical power of 80% or higher. Our post-hoc analysis demonstrates a statistical power of 85%.

In terms of neuron count, we recorded 11-83 neurons expressing GCaMP6m for the

mPFC→BLA group (with an average of 38) and 18-54 for the mPFC→NAc group (with an average of 39). This range was influenced by various factors, including the injected volume of viral GCaMP6m, expression levels, and the efficiency of Cre-mediated recombination. Following the data processing phase, which involved the identification of neurons through principal component and independent component analyses (PCA-ICA), approximately 1-9% of the identified components were identified as artifacts and subsequently excluded. The remaining components were classified as neurons and employed for subsequent analyses.

Behavioral tests

The behavioral tests spanned three consecutive days, maintaining consistent schedules throughout. To ensure cleanliness, the chamber was meticulously cleaned with 70% ethanol between trials. The Topscan behavior analysis system from Clever Sys, VA, was employed to monitor the animals' behaviors. This system also sent a TTL signal at the start of each test to trigger the microscope recording of neuronal activity.

Modified Three-Chamber (mTC) Test

The mTC test adhered to a previously established protocol (31) with several enhancements. The conventional three-chamber apparatus was transformed into a single open box (45 x 10 x 20 cm) featuring two small removable lateral chambers (10 x 10 x 40 cm). These chambers were separated by thin, spaced metal wires, permitting mice to interact with stimuli. Before the test, the subject mouse underwent a 10-minute habituation period within the open box devoid of stimuli. During testing, an age- and weight-matched, unfamiliar same-sex conspecific (referred to as the first social stimulus, M1) and an inanimate object (non-social stimulus, O) were randomly placed into the two lateral chambers. Subsequently, the subject mouse was positioned in the center of the open box and allowed to explore freely during a 10-minute testing session. Several behavioral parameters were assessed, including time spent in social interaction, object interaction, the social zone (SZ), the object zone (OZ), the transition zone, and grooming behavior.

Open field test (OFT)

The test was modified from a previous report (10). It was conducted in a square box (dimensions: 50 × 50 × 50 cm). The mouse was gently placed in the central field and allowed to explore freely during a 10-minute testing session. Locomotor activity was recorded by a camera. The center is defined as the central 25 cm x 25 cm square area, while the corner is a sector area with a 12.5 cm radius in each corner. Total distance traveled and time spent in each area, sniffing, and grooming behaviors were analyzed.

Elevated plus maze (EPM) test

It was conducted as previously described (32). The EPM apparatus, 40 cm high from the floor, consists of two open arms (35 × 10 cm) and two closed arms (35 × 10 cm), those two parts stretch perpendicular to each other and connect in a center platform (5 cm). Mice were placed in the center zone facing an open arm and allowed to explore the maze freely for 10 min. The time spent in open arms, closed arms, and behaviors of headdipping, sniffing, and grooming were analyzed.

Dominance tube test

The tube test protocol was modified from Wang et al (21). In brief, a clear acrylic tube with a 30 cm length and 2.8 cm inside diameter in which one mouse can pass or backward through the tube fluently but can't make a U-turn or climb through another mouse. The mice underwent a three-day training in which all mice went through the tube ten times per day, five times from each side without another competitor in the tube. The training procedure allows the mice to adapt to the test procedure and environment. The mice, in a very rare case, cannot be trained and were excluded for further testing. In the testing procedure, tests were conducted in a pair-wise style, and the number of times won by individual animals was recorded to determine the hierarchical ranking. The mouse who forced its competitor out of the tube was declared the "winner", or dominant in this situation. The mouse that was retreated is then designated the "loser", or subordinate. In most cases, the competition was completed within 2 minutes, or the tests were repeated. The rank is considered stable without ranking change in all mice for at least five consecutive days. Groups were categorized as "non-stable ranking" if they did not form a stable

ranking within 2 weeks. We single housed the mice for 5 days and subjected them to a round-robin tube test tournament (three trials per day for 7 trials) to determine social ranking. Twenty-four hours following the last tube test, the mice were subjected to other behavioral tests or in vitro studies, as described in the results.

Behavior data analysis

Behavioral data was meticulously tracked through aerial videography from an overhead perspective utilizing the Topscan behavioral data acquisition software (CleverSys, Reston, VA). This software allowed for the precise tracking and definition of the 2D locations of mice in various areas, including the OF center, corner area, EPM open-P, open-NP, closed-P, closed-NP arms, and mTC social zone, object zone, and middle zone. Additionally, specific behaviors such as sniffing, grooming, head-dipping, and social/object interaction were recognized and quantified by the software.

Ca^{2+} imaging with Miniature microscope

Imaging of freely moving mice was conducted using a head-mounted miniaturized microscope (nVista HD 2.0.4, Inscopix, Palo Alto, CA), as depicted in Figure 1A. This microscope was synchronized with the Topscan system through a TTL pulse, enabling simultaneous acquisition of Ca^{2+} signals and behavioral video. Prior to imaging, the microscope was securely affixed to the mouse's head. The imaging data were obtained at a frame rate of 15 Hz with a resolution of 1024 x 1024 pixels. LED power settings ranged from 0.3 to 1 mW, while gain settings were adjusted to 1 to 2 based on fluorescence intensity. Importantly, each individual mouse utilized the same imaging parameters consistently across all three experimental sessions.

Histology

Recording sites were meticulously validated through histological examination of lesions created during the lens implantation procedure. Mice were anesthetized via intraperitoneal injection, employing a combination of ketamine (400 mg/kg) and xylazine (20 mg/kg). Following this, transcardial perfusion was conducted using a phosphate buffer solution (PBS), followed by 4% paraformaldehyde (PFA). The brains of the mice, complete with their skulls and baseplates, were

post-fixed with 4% PFA for 3 days. Subsequently, the brains were extracted and sectioned into slices measuring 50-100 µm using a vibrating slicer (Vibratome Series 1000, St. Louis, MO). These sections were then mounted onto slides. To label cell nuclei, slides were subjected to incubation and storage in a 1:1000 Hoechst solution in 1x PBS (Invitrogen, Carlsbad, CA). Brain slides were meticulously imaged to precisely determine the placement of the GRIN lens and the extent of viral expression. This imaging process was conducted employing a Confocal Microscope (Zeiss LSM 710, Oberkochen, Germany).

Ca^{2+} image processing

Ca^{2+} images were processed offline using Inscopix Data Processing software (version 1.3.1). In brief, frames collected within a single day were concatenated into a stack and subsequently subjected to preprocessing, spatial filtering, and motion correction. To normalize the Ca^{2+} signal, the average projection of the filtered video was established as the background fluorescence (F_0). Instantaneous normalized Ca^{2+} fluorescent signals (ΔF/F) was calculated according to the formula, $(\Delta F/F)_i=(F_i-F_0)/F_0$, where i represents each frame. Individual cells were then identified using the principal component and independent component (PCA-ICA) analyses with no spatial or temporal down-sampling. Regions of interest (ROI) were selected based on signal and image criteria, with any components that did not correspond to single neurons being discarded.

Time-stamped traces of neurons were exported into data files formatted for custom-written Python scripts used for subsequent analysis. Ca^{2+} transients (events) were identified for each cell using a peak-finding algorithm, and frequency (transient rate) and amplitude (ΔF/F) data were processed using custom-written scripts. When analyzing frequency or amplitude changes in response to mouse behavior or location, frames of image and behavioral data were aligned and marked with corresponding behavioral event labels. For neuronal activity normalization, we employed the min-max normalization method to scale values between 0 and 1. In this method, the maximum neuron activity value was transformed into 1, while all other values were scaled to decimals between 0 and 1 using the equation: $z_i = \frac{x_i - min_{(x)}}{max_{(x)} - min_{(x)}}$, where x=(x1,x2,...,xn) represents an array of neuron frequency or amplitude values, and z_i denotes the normalized value.

Identification of location-modulated neural ensembles

To identify location-modulated neural ensembles in each session, we assessed each neuron's response preference to a specific location exploration. Initially, we computed the actual similarity (Sa) between the Ca^{2+} trace vectors (c_k) and behavior events (b), using the formula: $2b \cdot c_k/(|b|^2 + |c_k|^2)$ (13). Then, the behavior vector was subjected to random shuffling to compute a new similarity (S) with a neural trace for a given neuron. This shuffling process was repeated 5000 times, generating an S distribution histogram. Neurons were classified as ON neurons if their Sa values exceeded the 99.95th percentile of the S distribution.

Following neuron identification, we calculated the proportions of different location-modulated ON neurons for each mouse. Simultaneously, the transient rate and amplitude of these neuron ensembles were computed for each mouse in each paradigm.

Neuron alignment between tests

To identify and compare the same neurons across tests conducted on different days, thus enabling cross-test comparisons, we implemented a global alignment procedure. Initially, we reconstructed neuron distribution images based on their pixel locations and shapes. Subsequently, we converted each neuron image into a vector format and assessed their similarity using cosine similarity, as indicated by the formula below. The two parameters, degree of rotation (A) and pixel shift (B) were iteratively adjusted to maximize the cosine similarity of image vectors between tests. Given that the images from all three tests were collected under identical settings, the scale for the neuron images remained constant and did not require adjustment. Through this multi-start method, we achieved the global optimal solution for the parameters. Ultimately, we determined the number of overlapping neuron images across tests, which was then used for subsequent comparative analyses.

$$\text{Similarity} = \cos(\theta) = \frac{\mathrm{A} \cdot \mathrm{B}}{\| \mathrm{A} \| \| \mathrm{B} \|}$$

Optogenetics and patch-clamp recording

Viral injection for optogenetics

We stereotaxically injected an AAV_2-CaMKIIα-hChR2(H134R)-EYFP (UNC virus core, 0.5 µl of 1.00 E13 viral genomes/ml) into mPFC bilaterally (relative to bregma: +1.9 mm AP; ±0.3 mm ML; -2.0 mm DV) using a Hamilton microsyringe (Model 1701N) and a WPI microsyringe pump mounted to a KOPF Model 940 Small Animal Stereotaxic Instrument.

After viral injection, mice were recovered for 2 weeks to allow for the AAVs' efficacy. We then retrograde tracing from the mPFC to the NAc and BLA in brain slices. After euthanasia using 2% isoflurane, the mice underwent transcardial perfusion with 4% PFA to fix the entire brain. After a 6-hour fixation period, 50 µm coronal slices, encompassing the mPFC, NAc, and BLA, were dissected using a vibratome (Leica VT-1000S) and collected in ice-cold PBS. These sections were transferred onto gelatin-coated slides (Thermo Fisher Scientific) and mounted onto cover slides (Electron Microscopy Sciences). Nuclei were labeled using Gold antifade reagent with DAPI (Invitrogen). Fluorescence images were captured and visualized at 10x and 20x magnification under a Leica microscope (DMRXA2, Leica Microsystems) equipped with a digital camera and imaging software.

Brain slice preparation.

The patch clamp test was conducted following the completion of the tube test. Mice were anesthetized with 2% isoflurane and subsequently decapitated. The brain skull was swiftly removed and immersed in an ice-cold cutting solution composed of the following concentrations (in mM): 205 sucrose, 5 KCl, 1.25 NaH_2PO_4, 5 $MgSO_4$, 26 $NaHCO_3$, 1 $CaCl_2$, and 25 glucose; with an osmolarity of 300-320 mOsm. The brain was then sliced into 300-µm coronal sections using a vibratome (Leica VT-1000S), encompassing the mPFC, NAc, and BLA.

Post-sectioning, slices were maintained in a normal artificial cerebrospinal fluid (ACSF) solution for whole-cell recording, containing the following concentrations (in mM): 115 NaCl, 2.5 KCl, 2 $CaCl_2$, 1 $MgCl_2$, 1.25 NaH_2PO_4, 17 glucose, 25 $NaHCO_3$; with an osmolarity of 280-300 mOsm. The slices were bubbled with 95% O_2 / 5% CO_2 for one hour at ambient temperature (22 ± 3°C).

Whole-cell patch-clamp recordings were conducted by placing the slices in a submerged recording chamber and perfusing them with ACSF at a rate of 1 ml/min.

Patch-clamp recording

The pipette solution for EPSC recordings contained (in mM): 145 Cs-methanesulfonate (Cs-SO_3CH_3), 8 NaCl, 1 $MgCl_2$, 0.38 $CaCl_2$, 1 Cs-EGTA, and 10 HEPES (mOsm 280 - 300, adjusted to pH 7.25 with CsOH). For action potential recordings, $CsSO_3CH_3$ was replaced by K-SO_3CH_3. The pipette resistance was 8-10 M ohm. Brain slices were recorded through an Axon Instruments Multiclamp 700B amplifier, sampled at 10 kHz, and digitized with a Digidata 1440A (Molecular Device software). The cell morphology was identified under an Olympus BX51 fluorescence microscope. 100 μM picrotoxin was included in the ACSF throughout the recording.

A blue light pulse (PlexBright LED, 470nm) was utilized to activate mPFC fibers expressing ChR2. To validate the expression of ChR2 in the mPFC, inward current in voltage-clamp recording was assessed at -80 mV for 1 second, with a light intensity of 1 μW. Furthermore, action potential firing was examined in current clamp mode at frequencies of 5, 10, and 20 Hz, induced by a 1 ms light pulse with an intensity of 1 μW.

To elicit synaptic responses in the NAc and BLA through light pulses targeting mPFC fibers, slices were illuminated at 30-second intervals, with a short duration of 1-5 ms for NAc neurons and 1-10 ms for BLA neurons. EPSCs were induced by incrementally increasing light intensity (1, 2, 5, and 10 μW) at a holding potential of -80 mV, normalized by dividing by the response at 10 μW. PPR responses at 50 and 75 ms intervals were measured at an intensity of 1 μW, and the amplitude of the second response was divided by that of the first response. To determine the AMPA/NMDA current ratio, current responses were recorded at a holding potential of –70 mV (AMPA) and +40 mV (NMDA), with an intensity of 2 μW.

Statistics

All statistical analyses were performed using SPSS (version 24, IBM, Armonk, NY), Excel (Microsoft, Redmond, WA), and Python custom scripts. Since all the data could pass the normal

distribution test (D'Agostino and Pearson), a two-tailed paired or unpaired t-test was applied for two-group comparison, whereas one-way ANOVA and multiple comparison test (Tukey) was used for multiple-group comparison. For multiple-factors comparison, two-way RM ANOVA was used, followed by Bonferroni-corrected post hoc comparisons. Statistical significance was taken as * $p < 0.05$, ** $p < 0.01$. All data are represented as mean ± SEM unless otherwise specified.

DATA AVAILABILITY

All data that support the findings in this study and the code used to analyze the data are available upon reasonable request.

ACKNOWLEDGEMENTS

This work was supported by the NIH grant R01NS118197, and the George Washington University 2018-2023 Cross-Disciplinary Research Fund to H. L. and R.S. / C. Z. The National Institutes of Mental Health (1R01MH113986), the Cystic Fibrosis Foundation (002544I221), and the University of Tennessee Health Science Center start-up fund to J.D.

AUTHOR CONTRIBUTIONS

H.L. and J.D. conceived the project. H.L., J.D., C.L., G.P., P. X., Q.G., and Z.J. designed the experiments. C.L. and P.X. performed the in vivo Ca^{2+} experiments. C.L., P.X., X.S., Y.L., R.S., and C.Z. performed imaging data analysis. Q.G. and Z.J. performed the behavior experiments. Z.J. performed mouse surgery for the optogenetic experiment. G.P. performed optogenetics and patch-clamp experiments and data analysis. X.L. and Q.L. performed histology. C.L., H.L., and J.D. wrote the manuscript. All authors reviewed and edited the manuscript.

CONFLICT OF INTEREST

The authors declare no competing financial interests.

ADDITIONAL INFORMATION

Supplementary information is available on AS's website.

REFERENCES

1. Floresco SB. The nucleus accumbens: an interface between cognition, emotion, and action. Annu Rev Psychol. 2015;66:25-52.
2. Salzman CD, Fusi S. Emotion, cognition, and mental state representation in amygdala and prefrontal cortex. Annu Rev Neurosci. 2010;33:173-202.
3. Pastor V, Medina JH. Medial prefrontal cortical control of reward- and aversion-based behavioral output: Bottom-up modulation. Eur J Neurosci. 2021;53(9):3039-62.
4. Ishikawa J, Sakurai Y, Ishikawa A, Mitsushima D. Contribution of the prefrontal cortex and basolateral amygdala to behavioral decision-making under reward/punishment conflict. Psychopharmacology (Berl). 2020;237(3):639-54.
5. Piantadosi PT, Yeates DCM, Floresco SB. Prefrontal cortical and nucleus accumbens contributions to discriminative conditioned suppression of reward-seeking. Learn Mem. 2020;27(10):429-40.
6. Diehl MM, Bravo-Rivera C, Quirk GJ. The study of active avoidance: A platform for discussion. Neurosci Biobehav Rev. 2019;107:229-37.
7. Mitchell JF, Sundberg KA, Reynolds JH. Spatial attention decorrelates intrinsic activity fluctuations in macaque area V4. Neuron. 2009;63(6):879-88.
8. Warlow SM, Naffziger EE, Berridge KC. The central amygdala recruits mesocorticolimbic circuitry for pursuit of reward or pain. Nat Commun. 2020;11(1):2716.
9. Kim CK, Ye L, Jennings JH, Pichamoorthy N, Tang DD, Yoo AW, et al. Molecular and Circuit-Dynamical Identification of Top-Down Neural Mechanisms for Restraint of Reward Seeking. Cell. 2017;170(5):1013-27 e14.
10. Prut L, Belzung C. The open field as a paradigm to measure the effects of drugs on anxiety-like behaviors: a review. Eur J Pharmacol. 2003;463(1-3):3-33.
11. Walsh RN, Cummins RA. The Open-Field Test: a critical review. Psychol Bull. 1976;83(3):482-504.
12. Kring DKaAM. Emotion, Social Function, and Psychopathology. Review of General Psychology. 1998;2(3):320-42.
13. Liang B, Zhang L, Barbera G, Fang W, Zhang J, Chen X, et al. Distinct and Dynamic ON and OFF Neural Ensembles in the Prefrontal Cortex Code Social Exploration. Neuron. 2018;100(3):700-14 e9.
14. Frost NA, Haggart A, Sohal VS. Dynamic patterns of correlated activity in the prefrontal cortex encode information about social behavior. PLoS Biol. 2021;19(5):e3001235.
15. Cohen MR, Maunsell JH. Attention improves performance primarily by reducing interneuronal correlations. Nat Neurosci. 2009;12(12):1594-600.
16. Friedrich RW, Wiechert MT. Neuronal circuits and computations: pattern decorrelation in the olfactory bulb. FEBS Lett. 2014;588(15):2504-13.

17. Xu P, Yue Y, Su J, Sun X, Du H, Liu Z, et al. Pattern decorrelation in the mouse medial prefrontal cortex enables social preference and requires MeCP2. Nat Commun. 2022;13(1):3899.

18. Adam C. Nelson VK, Eric Vaughn, Jeshurun A. Gnanasegaram, Nimrod D. Rubinstein, Venkatesh N Murthy, Catherine Dulac. Molecular and Circuit Architecture of Social Hierarchy. bioRxiv. 2019.

19. Fan Z, Zhu H, Zhou T, Wang S, Wu Y, Hu H. Using the tube test to measure social hierarchy in mice. Nat Protoc. 2019;14(3):819-31.

20. Kingsbury L, Huang S, Wang J, Gu K, Golshani P, Wu YE, et al. Correlated Neural Activity and Encoding of Behavior across Brains of Socially Interacting Animals. Cell. 2019;178(2):429-46 e16.

21. Wang F, Zhu J, Zhu H, Zhang Q, Lin Z, Hu H. Bidirectional control of social hierarchy by synaptic efficacy in medial prefrontal cortex. Science. 2011;334(6056):693-7.

22. Zhou T, Zhu H, Fan Z, Wang F, Chen Y, Liang H, et al. History of winning remodels thalamo-PFC circuit to reinforce social dominance. Science. 2017;357(6347):162-8.

23. Berridge KC, Kringelbach ML. Pleasure systems in the brain. Neuron. 2015;86(3):646-64.

24. Ikemoto S. Dopamine reward circuitry: two projection systems from the ventral midbrain to the nucleus accumbens-olfactory tubercle complex. Brain Res Rev. 2007;56(1):27-78.

25. Davis M. The role of the amygdala in fear and anxiety. Annu Rev Neurosci. 1992;15:353-75.

26. LeDoux JE. Emotion circuits in the brain. Annu Rev Neurosci. 2000;23:155-84.

27. Robbins TW, Everitt BJ. Neurobehavioural mechanisms of reward and motivation. Curr Opin Neurobiol. 1996;6(2):228-36.

28. Schultz W. Behavioral dopamine signals. Trends Neurosci. 2007;30(5):203-10.

29. Phelps EA, LeDoux JE. Contributions of the amygdala to emotion processing: from animal models to human behavior. Neuron. 2005;48(2):175-87.

30. Tovote P, Fadok JP, Luthi A. Neuronal circuits for fear and anxiety. Nat Rev Neurosci. 2015;16(6):317-31.

31. Lee E, Rhim I, Lee JW, Ghim JW, Lee S, Kim E, et al. Enhanced Neuronal Activity in the Medial Prefrontal Cortex during Social Approach Behavior. J Neurosci. 2016;36(26):6926-36.

32. Walf AA, Frye CA. The use of the elevated plus maze as an assay of anxiety-related behavior in rodents. Nat Protoc. 2007;2(2):322-8.

Fig. 1

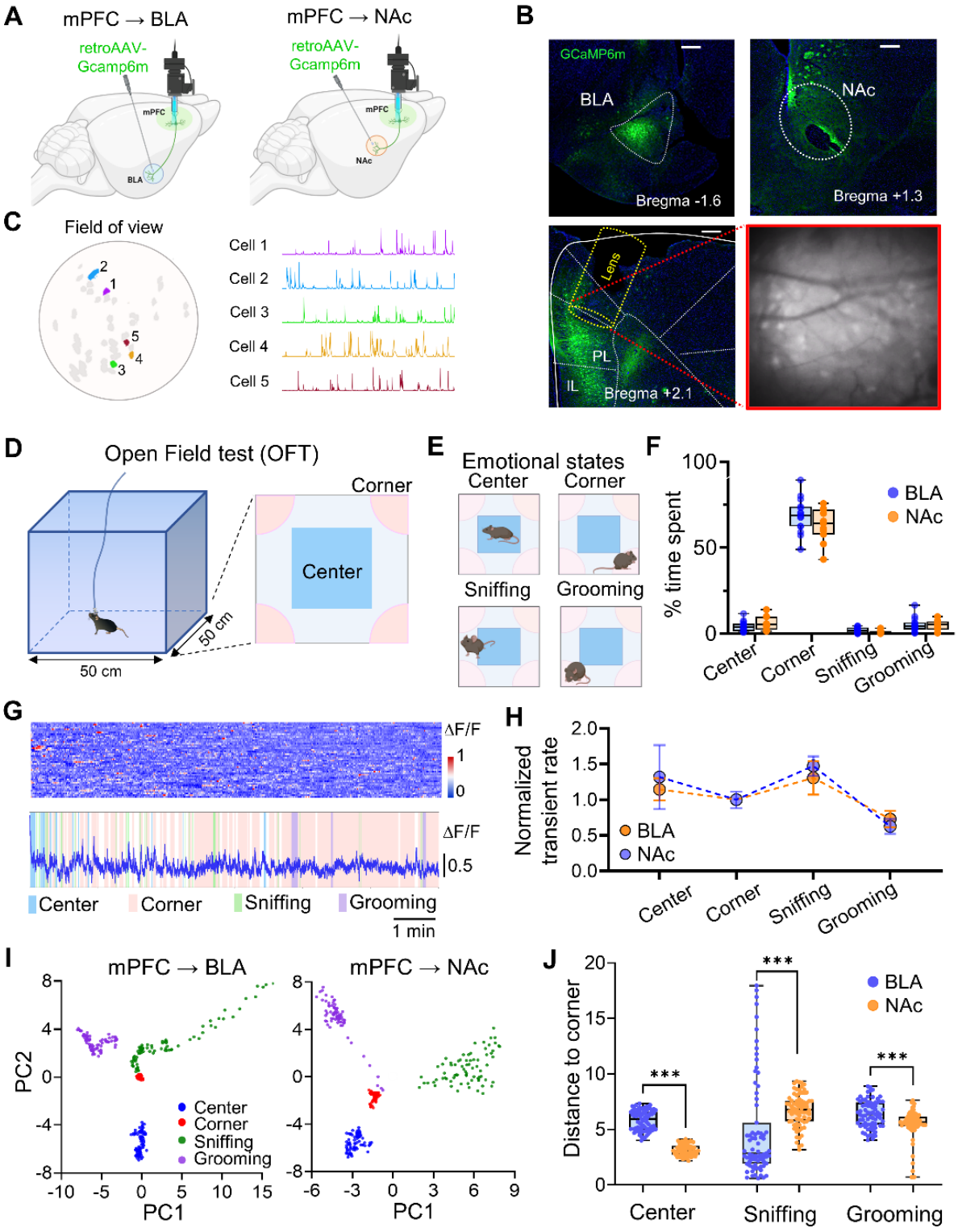
A
mPFC → BLA
retroAAV-Gcamp6m
mPFC
BLA
mPFC → NAc
retroAAV-Gcamp6m
mPFC
NAc
B
GCaMP6m
BLA
Bregma -1.6
NAc
Bregma +1.3
Lens
PL
IL
Bregma +2.1
C
Field of view
Cell 1
Cell 2
Cell 3
Cell 4
Cell 5
D
Open Field test (OFT)
Corner
Center
50 cm
50 cm
E
Emotional states
Center
Corner
Sniffing
Grooming
F
% time spent
BLA
NAc
Center
Corner
Sniffing
Grooming
G
ΔF/F
ΔF/F
0.5
Center
Corner
Sniffing
Grooming
1 min
H
Normalized transient rate
BLA
NAc
Center
Corner
Sniffing
Grooming
I
mPFC → BLA
mPFC → NAc
PC2
PC1
PC1
Center
Corner
Sniffing
Grooming
J
Distance to corner
BLA
NAc
***
***
***
Center
Sniffing
Grooming

Figure 1. The mPFC→NAc and mPFC→BLA neurons demonstrated distinct activity patterns across various emotional states.

(A) Schematic showing retrograde AAV-GCaMP6 injection in the NAc and BLA, respectively. In vivo Ca^{2+} imaging was performed in the mPFC neurons expressing GCaMP6 via miniscope.

(B) Top: An example of AAVretro-GCaMP6 injection and expression in the BLA and NAc, respectively. Bottom: An example of GCaMP6m expression in the mPFC with AAVretro-GCaMP6 injection in the NAc and an image of Ca^{2+} fluorescence recorded with the miniaturized microscope. Green, GCaMP6m. Scale bars, 200 mm.

(C) Left: the field of view under a GRIN lens in one mouse with identified neurons numbered and colored. Right: fluorescence traces of example neurons marked in the above panel.

(D) Schematic of the open field test (OFT) in an open 50 cm X 50 cm arena. The green areas represent corners and the orange area represents the center.

(E) Illustrations depicting typical mouse behaviors associated with different emotional states observed during the OFT: Center (exploration and higher anxiety), Corner (lower anxiety), sniffing (sensory exploration and vigilance, possibly indicating curiosity, cautious exploration, or heightened alertness), and grooming (stress relief or comfort).

(F) The percentage of time that mice spent in the center, corners, sniffing, and grooming during a 10-min open field test. n = 15 mice for mPFC→BLA group; n = 11 mice for mPFC→NAc group. The behavioral performance between these two groups of mice showed no significant difference.

(G) Heatmap and time-series plot of neuronal activity ($\Delta F/F$) across the test duration. The heatmap above shows the fluctuation in activity level across neurons, while the plot below aligns the averaged fluctuations of these neurons with observed behaviors (Center, Corner, Sniffing, Grooming) within the arena.

(H) Normalized transient rates of neuronal activity during different behaviors. Both mPFC→BLA and mPFC→NAc pathways are plotted, indicating no significant variation in neuronal firing rates across behaviors.

(I) PCA plots for mPFC→BLA and mPFC→NAc pathways illustrating the distribution of neuronal activity patterns for different observed behaviors (Center: blue, Corner: red, Sniffing: green, Grooming: purple). Each point represents an individual neuronal recording.

(J) Summary of the distances of neuronal activity clusters from the center of Corner behavior in the OFT for both pathways

Data are represented as mean ± SEM. * $p < 0.05$, *** $p < 0.001$, Mann-Whitney U test.

Fig. 2

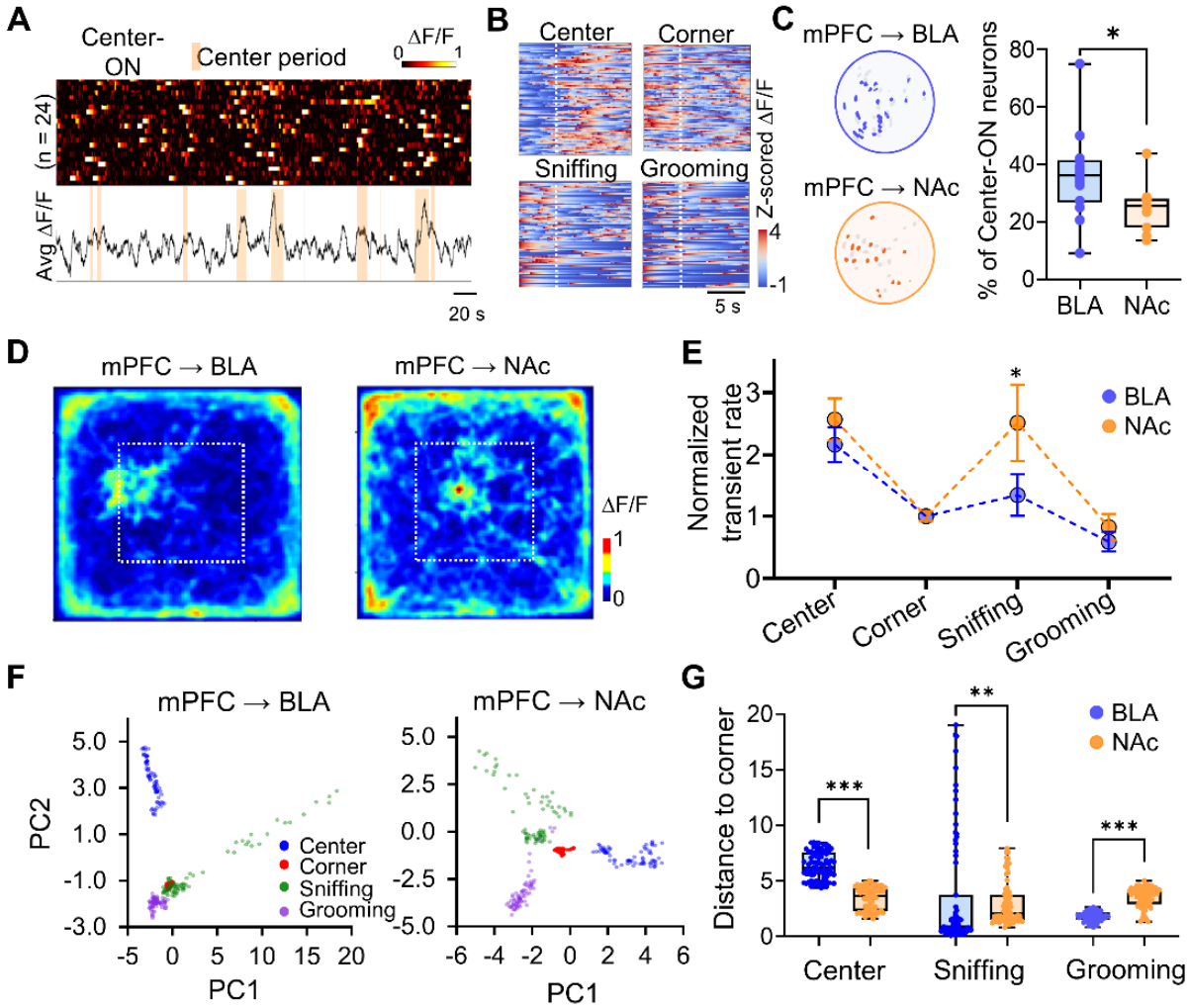

Figure 2. Distinct encoding of emotional status by center-ON neurons in the mPFC pathways

(A) Ca^{2+} traces of the averaged activity of center-ON neuron ensembles around the onset of center entry (5 s before to 5 s after). Solid lines represent the averaged value and shaded regions indicate SEM.

(B) Heatmaps depicting the activity patterns of neurons across four different behavioral contexts: Center, Corner, Sniffing, and Grooming. Each column corresponds to a different behavior, with the intensity of color indicating the level of neuronal activity.

(C) Left: spatial distributions of center-ON neurons among the mPFC→BLA and mPFC→NAc neurons in one representative mouse from each group. Right: the percentage of center-ON neurons within the mPFC→BLA and mPFC→NAc neuron ensembles.

(D) Spatial heatmaps of neuronal activity across the open field arena of all observed center-ON neurons in one example mouse of mPFC→BLA and mPFC→NAc groups. The color bar indicates the averaged normalized z-score.

(E) Averaged transient rate in four different states during the OFT.

(F) PCA plots illustrating the distribution of neuronal activity patterns during different behaviors for mPFC→BLA and mPFC→NAc pathways. Points are color-coded by behavior type (Center: blue, Corner: red, Sniffing: green, Grooming: purple).

(G) Summary of the distances from the center of Corner behavior in terms of neuronal activity for each behavior in both mPFC pathways.

Data are represented as mean ± SEM. * $p < 0.05$, ** $p < 0.01$, *** $p < 0.001$, Mann-Whitney U test.

Fig. 3

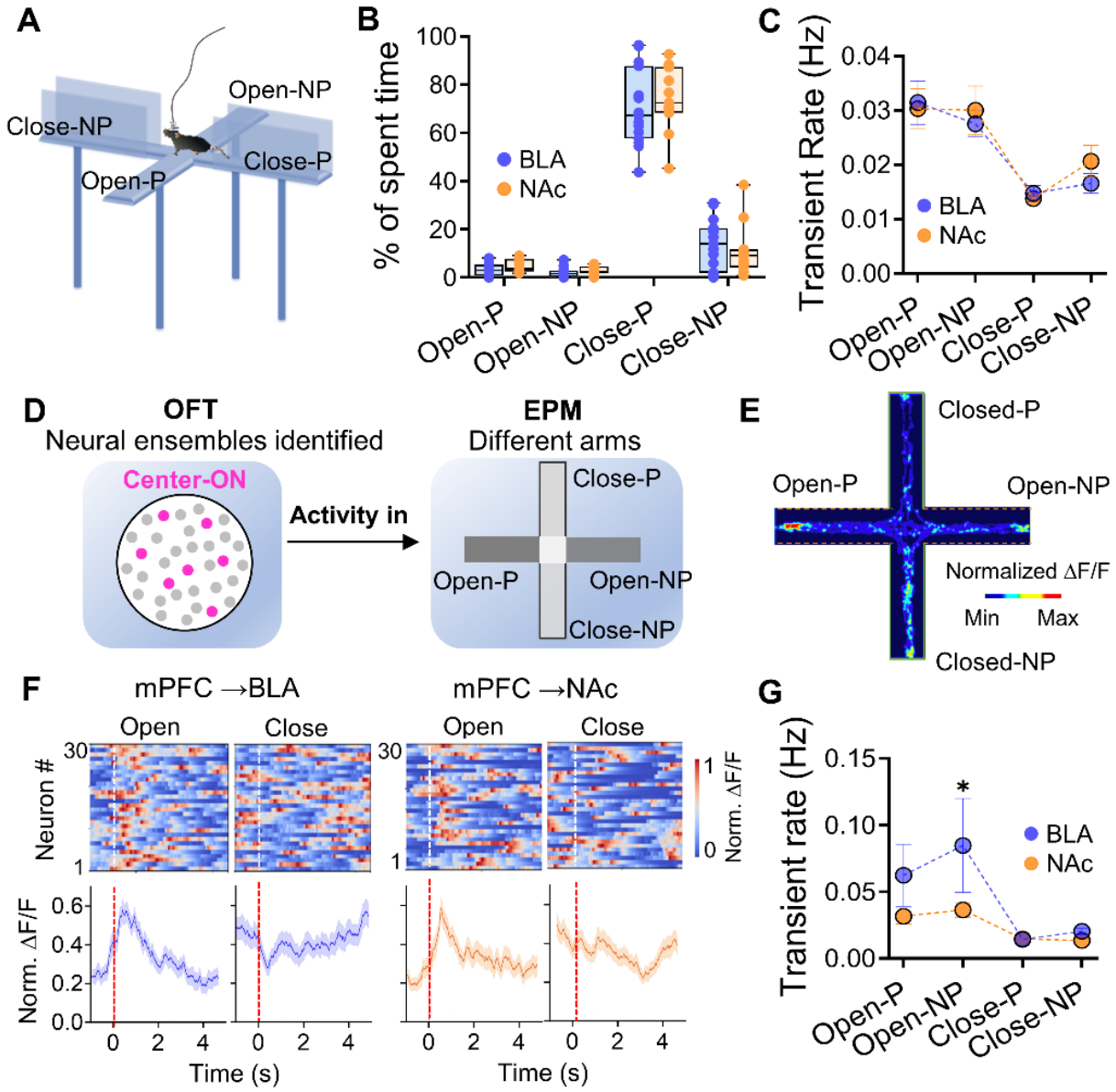

Figure 3. The mPFC→NAc and mPFC→BLA neurons demonstrated distinct activity patterns across various emotional states during the EPM test.

(A) Schematic illustration of the Elevated Plus Maze (EPM) test setup showing the layout of open (Open-P, Open-NP) and closed (Close-P, Close-NP) arms used to assess anxiety-related behaviors in mice.

(B) Box plots displaying the percentage of time spent by mice in the different arms of the EPM (Open-P, Open-NP, Close-P, Close-NP) for both mPFC→BLA and mPFC→NAc pathways. Data indicate variations in time spent across different arms, highlighting behavioral preferences.

(C) Averaged transient rates (Hz) of neuronal activity of all recorded neurons in the mPFC→BLA and mPFC→NAc pathways in each arm of the EPM. Neuronal activity patterns are compared across these two pathways, showing no significant difference.

(D) Analysis design of observing the neural activities of center-ON ensembles of OFT in different EPM arms.

(E) Mean Ca^{2+} signal across the EPM arms of all observed center-ON neurons in one example mouse. The color bar indicates the averaged normalized z-score.

(F) Example 30 center-ON neurons (top) and corresponding averaged activity (bottom) around the onset of arm entry during the EPM test. Time 0 represents the onset of arm entry.

(G) Averaged transient rate in four different arms during the EPM test. n = 9-13 mice mPFC→BLA group; n = 5-8 mice for mPFC→NAc group.

Data are represented as mean ± SEM. * $p < 0.05$, Mann-Whitney U test.

Fig. 4

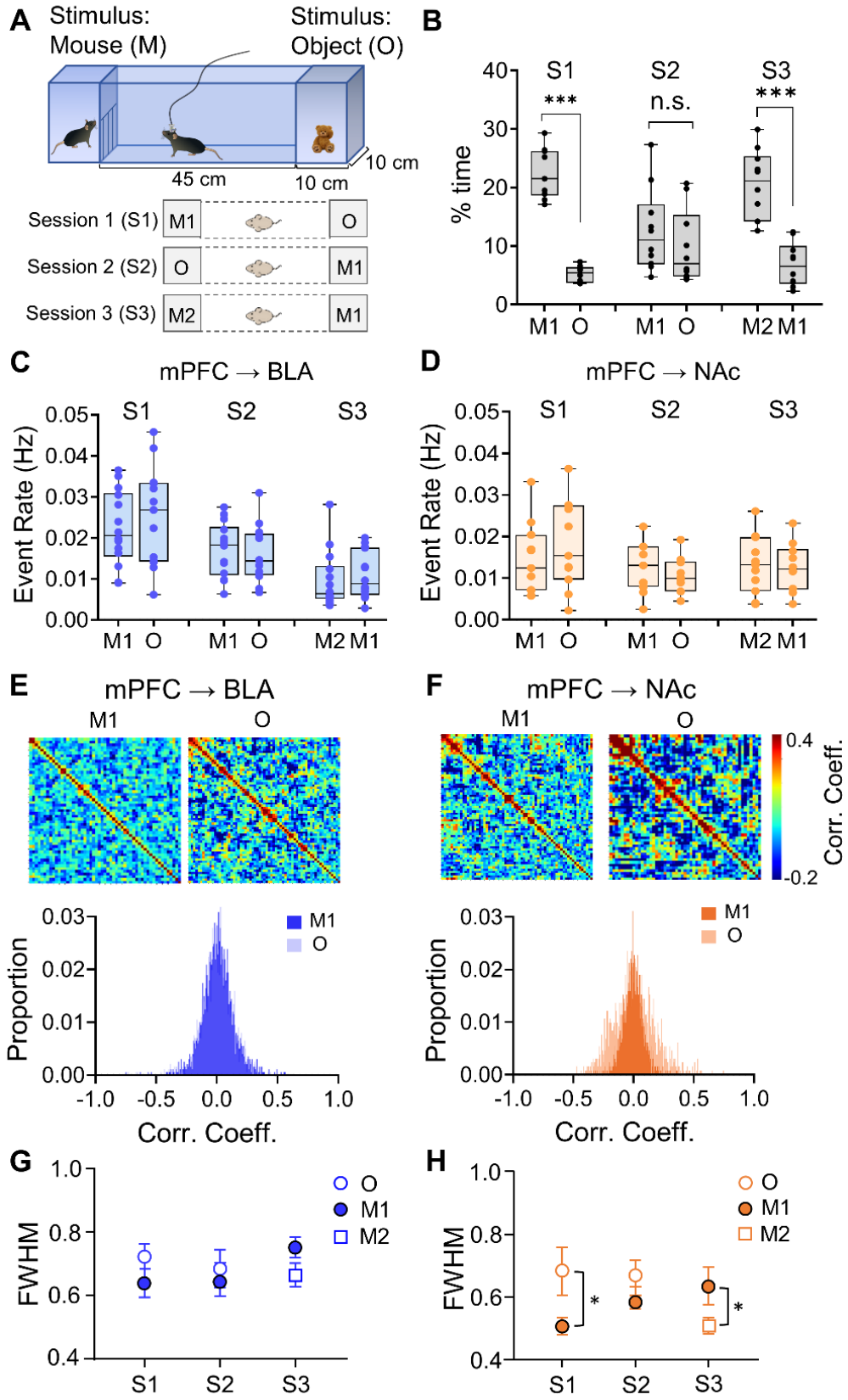
A
Stimulus: Mouse (M)
Stimulus: Object (O)
45 cm
10 cm
10 cm
Session 1 (S1) M1 O
Session 2 (S2) O M1
Session 3 (S3) M2 M1
B
S1
S2
S3
***
n.s.
***
% time
M1 O M1 O M2 M1
C
mPFC → BLA
Event Rate (Hz)
S1 S2 S3
M1 O M1 O M2 M1
D
mPFC → NAc
Event Rate (Hz)
S1 S2 S3
M1 O M1 O M2 M1
E
mPFC → BLA
M1
O
Proportion
M1
O
Corr. Coeff.
F
mPFC → NAc
M1
O
0.4
-0.2
Corr. Coeff.
Proportion
M1
O
Corr. Coeff.
G
FWHM
O
M1
M2
S1 S2 S3
H
FWHM
O
M1
M2
*
*
S1 S2 S3

Figure 4. Pattern decorrelation is shown by the mPFC→NAc neurons, but not mPFC→BLA neurons.

(A) Top: the apparatus for the social interaction test. The subject mouse is in the middle 45 cm-long chamber; the 10 cm end compartments contain different stimuli. Bottom: the three sessions of the social interaction test. In the first 10-minute test session (S1), a strange mouse (M1) and an object (O) were placed in the end chambers; session 2 (S2) used the same stimuli but swapped their positions; in session 3 (S3) a new mouse (M2) replaced O, so that the subject mouse must choose whether to interact with a familiar or strange mouse (M1 vs. M2).

(B) The percentage of time that mice (n = 10) spent interacting with stimuli in each session.

(C-D) The averaged Ca^{2+} event rate when mice were engaged with different stimuli over the three sessions. n = 14 mice mPFC→BLA group; n = 11 for mPFC→NAc group. Data are represented as mean ± SEM. The event rates during interaction with M1 and O did not show statistical significance across all three sessions for both the mPFC→BLA and mPFC→NAc groups, two-way RM-ANOVA with Bonferroni–corrected post hoc comparisons.

(E-F) Top: raster plots of correlation coefficient of paired mPFC neurons during interactions with different stimuli, from a representative mouse in mPFC→BLA and mPFC→NAc group, respectively. Bottom: distribution of pair-wise Pearson correlation coefficients among these recorded mPFC neurons in responding to stimuli in each session. The blue and orange plots represent M1 interactions, while the lighter colors represent the interaction with the other stimulus (O).

(G) The averaged full width at half maximum (FWHM) of correlation coefficient distribution of individual mice in mPFC→BLA (n = 11) and mPFC→NAc (n = 10) group during interactions with different stimuli.

Data are represented as mean ± SEM. * $p < 0.05$, *** $p < 0.001$, Mann-Whitney U test.

Fig. 5

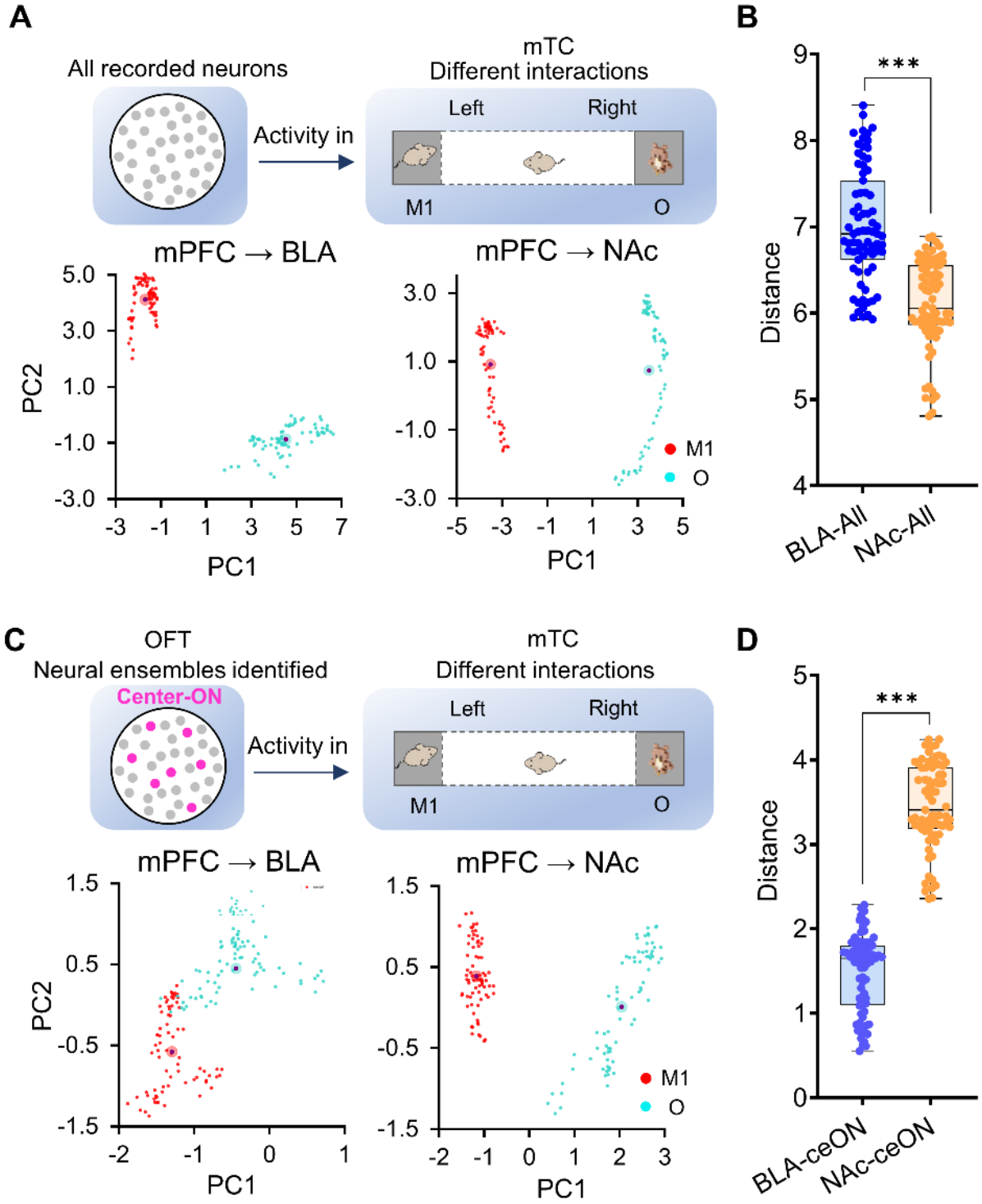
A
All recorded neurons
Activity in
mTC
Different interactions
Left
Right
M1
O
mPFC → BLA
mPFC → NAc
PC2
PC1
M1
O
B
***
Distance
BLA-All
NAc-All
C
OFT
Neural ensembles identified
Center-ON
Activity in
mTC
Different interactions
Left
Right
M1
O
mPFC → BLA
mPFC → NAc
PC2
PC1
M1
O
D
***
Distance
BLA-ceON
NAc-ceON

Figure 5. Comparative analysis of all neurons and center-ON subsets reflects divergent encoding patterns in the mPFC→BLA and mPFC→NAc Pathways.

(A) PCA plots showing the activity of all recorded neurons in the mPFC→BLA and mPFC→NAc pathways during interactions with a social stimulus (mouse, M1) and a nonsocial stimulus (object, O) in a modified Three Chamber Test (mTC). The plots reveal distinct clustering of neural activity patterns for each stimulus within both pathways.

(B) Distances between all neuronal activity clusters for nonsocial (O) interactions from the center of that for M1 interaction, compared across mPFC→BLA and mPFC→NAc pathways. Significant difference is demonstrated in the mPFC→BLA pathway.

(C) PCA plots for center-ON neurons identified during the Open Field Test (OFT). These plots illustrate the activity of these neurons in the mPFC→BLA and mPFC→NAc pathways during the same social and nonsocial stimuli. Clusters show how Center-ON neurons specifically respond to each type of stimulus.

(D) Distances of all center-ON neuronal activity clusters from the center of that for M1 interaction, compared across mPFC→BLA and mPFC→NAc pathways. Significant difference is demonstrated in the mPFC→NAc pathway.

Data are represented as mean ± SEM. *** $p < 0.001$, Mann-Whitney U test.

Fig. 6

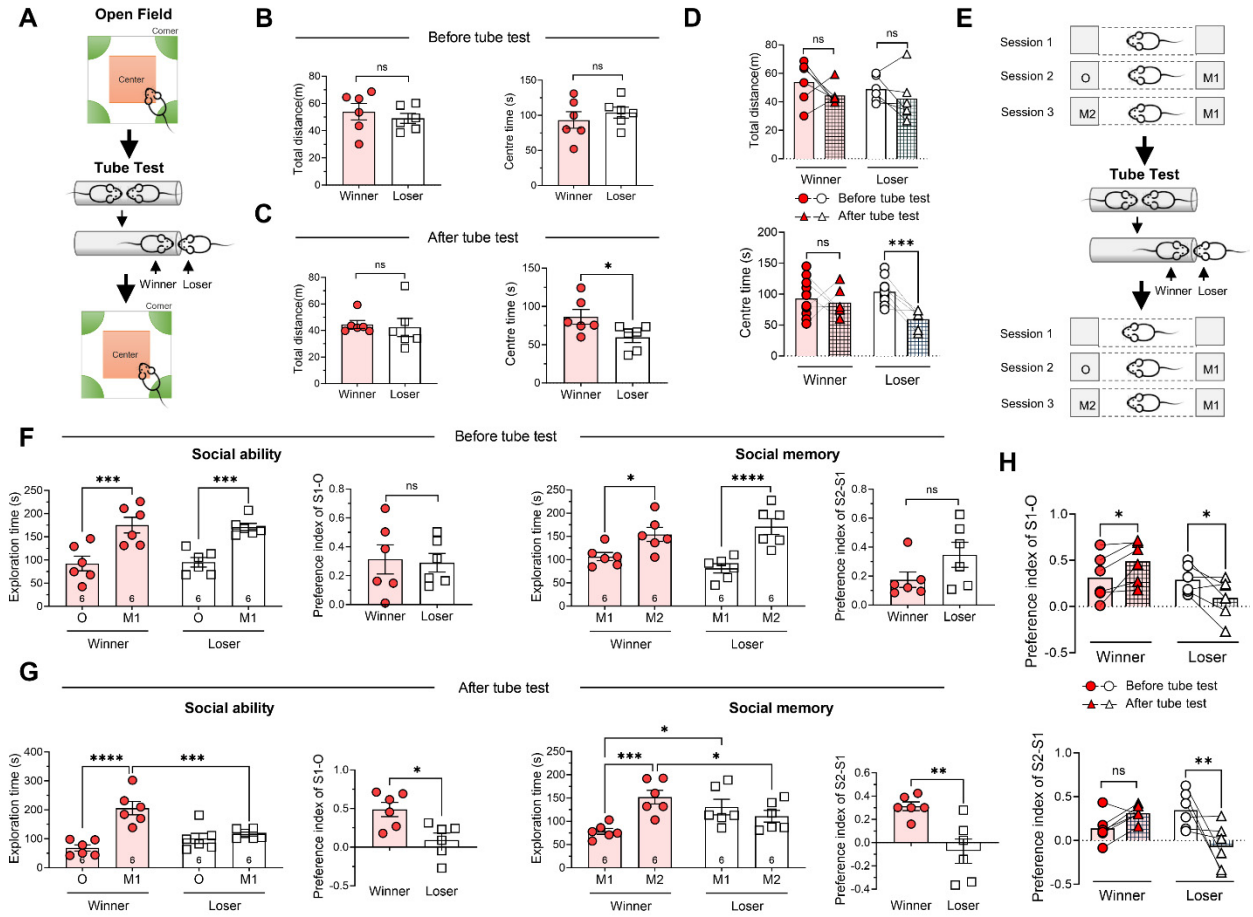

Figure 6. The modifications in the social ranking of mice alter their anxiety and social states.

(A) Schematic illustrating the experimental scheme. Mice underwent an open field test, followed by five consecutive days of tube tests (once daily) to establish their social rankings. Subsequently, both the winner and loser mice underwent a repeat open field test to assess their anxiety states.

(B-C) The mice's total distance traveled in the open field and time spent in the center zones before and after the tube test. * $p < 0.05$; ns, non-significant. n = 6 mice for each group, winner vs loser, unpaired Student's t-test.

(D) The differences in total distance (top) and center time (below) between winner and loser groups before and after the tube tests. *** $p < 0.001$; ns, non-significant. Before vs. after tube test, Two-way ANOVA Multiple comparisons, Sidak's post-hoc test.

(E) Schematic illustrating the three-chamber test for social ability and social memory. Mice were introduced to the middle chamber, which comprised two smaller side chambers, and underwent three 10-minute sessions. In Session 1, mice acclimated to the apparatus without the presence of another mouse or object (O). For the social ability test (session 2), a novel mouse (M1) occupied one side chamber, while an object was placed in the other. In the

social memory test (session 3), the previously encountered mouse (M1) remained in one side chamber, while a new mouse (M2) replaced the object in the other side chamber. After the three-chamber test, the mice underwent tube tests to establish their social rankings followed by a repeat three-chamber test to assess their social states.

(F) The mice's exploration time near M1 and O/M2 during the social ability test (left) and social memory test (right) conducted before the tube test. Social ability index calculated as (time near M1 chamber - time near object chamber) / (time near M1 chamber + time near object chamber). The social memory index is calculated as (time near M2 chamber - time near M1 chamber) / (time near M2 chamber - time near M1 chamber). * $p < 0.05$, *** $p < 0.001$, **** $p < 0.0001$, ns, non-significant. Two-way ANOVA Multiple comparisons, Sidak's post-hoc test. Unpaired Student's t-test for preference index.

(G) The mice's exploration time was spent near the M1 and O/M2 during the social ability test and social memory test after the tube test. * $p < 0.05$, *** $p < 0.001$, **** $p < 0.0001$. Two-way ANOVA Multiple comparisons, Sidak's post-hoc test. Unpaired Student's t-test for preference index.

(H) The comparisons of the social ability index (top) and social memory index (below) of the winner and loser group before and after the tube tests. * $p < 0.05$, ** $p < 0.01$, *** $p < 0.001$, ns, non-significant. Two-way ANOVA Multiple comparisons, Sidak's post-hoc test). n = 6 mice for each group.

Fig. 7

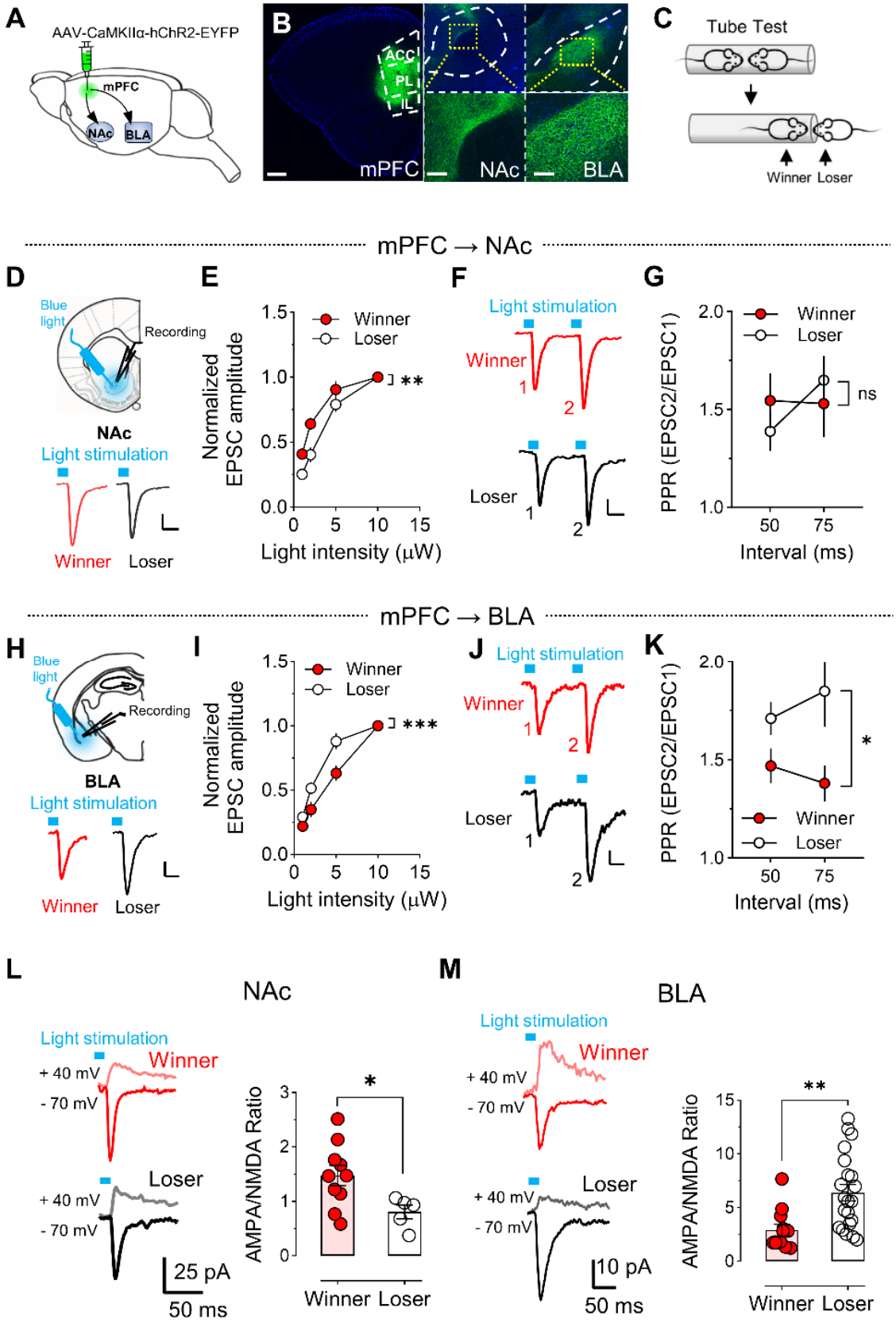
A
AAV-CaMKIIα-hChR2-EYFP
mPFC
NAc
BLA
B
ACC
PL
IL
mPFC
NAc
BLA
C
Tube Test
Winner
Loser
mPFC → NAc
D
Blue light
Recording
NAc
Light stimulation
Winner
Loser
E
Winner
Loser
Normalized EPSC amplitude
**
Light intensity (μW)
F
Light stimulation
Winner
Loser
G
Winner
Loser
PPR (EPSC2/EPSC1)
ns
Interval (ms)
mPFC → BLA
H
Blue light
Recording
BLA
Light stimulation
Winner
Loser
I
Winner
Loser
Normalized EPSC amplitude
***
Light intensity (μW)
J
Light stimulation
Winner
Loser
K
Winner
Loser
PPR (EPSC2/EPSC1)
*
Interval (ms)
L
NAc
Light stimulation
Winner
+ 40 mV
- 70 mV
Loser
+ 40 mV
- 70 mV
25 pA
50 ms
AMPA/NMDA Ratio
*
Winner
Loser
M
BLA
Light stimulation
Winner
+ 40 mV
- 70 mV
Loser
+ 40 mV
- 70 mV
10 pA
50 ms
AMPA/NMDA Ratio
**
Winner
Loser

Figure 7. The social status-dependent PL-NAc and PL-BLA neuronal activities.

(A) Schematic showing the AAV-ChR2 injection in the PL of mPFC.

(B) Expression of ChR2-EYFP in the mPFC, and terminal expression of ChR2-EYFP in the NAc and BLA. Scale bar, 400 μm, 50 μm, and 50 μm, from left to right.

(C) The ChR2-EYFP expressed mice underwent the tube test to determine their winner and loser status.

(D) The EPSCs in the NAc were evoked by 470 nM blue light. Upper, schematic showing the light fiber placement and EPSC recording sites in the NAc; Lower, representative EPSCs in the brain slices from the winner (red) and loser (black) mice. Scale bar, 30 pA and 25 ms.

(E) The normalized light intensity-dependent EPSCs. The data points were normalized to 10 μW and were shown as mean values. Winner, n= 19 neurons/ 7 mice; Loser n= 14 neurons/ 7 mice.

(F) The representative pair pulse ratio (PPR) of the EPSCs in the NAc (the light intensity was 1-2 μW and the interpulse interval was 50 and 75 ms). Scale bar, 8 pA and 25 ms.

(G) Summarized plots of the PPR under different interpulse intervals. Winner, n= 7 neurons/ 7 mice; Loser, n = 14 neurons/ 7 mice. ns, non-significant. Scale bar, 8 pA and 25 ms.

(H-I) EPSC recordings in the BLA. Winner, n = 17 neurons/ 7 mice; Loser n = 21 neurons/ 7 mice. Scale bar, 6 pA and 25 ms.

(J) The representative PPR of the EPSCs in the BLA.

(K) Summarized plots of the PPR under different interpulse intervals. Winner, n = 8 neurons/ 7 mice; Loser, n = 11 neurons/ 7 mice. Scale bar, 3 pA, and 25 ms.

(L) Left, representative EPSCs in the PL-NAc neurons from winner (red) and loser (black) mice. Right, the summarized AMAP/NMDA ratio. Winner, n= 5 neurons/ 5 mice; Loser n= 7 neurons/ 7 mice, 1-5 ms pulse). Scale bar, 25 pA and 50 ms.

(M) Left, representative EPSCs in the PL-BLA neurons from winner (red) and loser (black) mice. Right, the summarized AMAP/NMDA ratio. Winner, n= 12 neurons/ 7 mice; Loser n= 21 neurons/ 7 mice, 1-10 ms pulse). Scale bar, 10 pA, and 50 ms.

Data are shown as mean ± SEM. * $p < 0.05$, ** $p < 0.01$, *** $p < 0.001$. Two-way ANOVA for C, G, I, and K; two-tailed paired Student's t-test for L and M.

Fig. 8

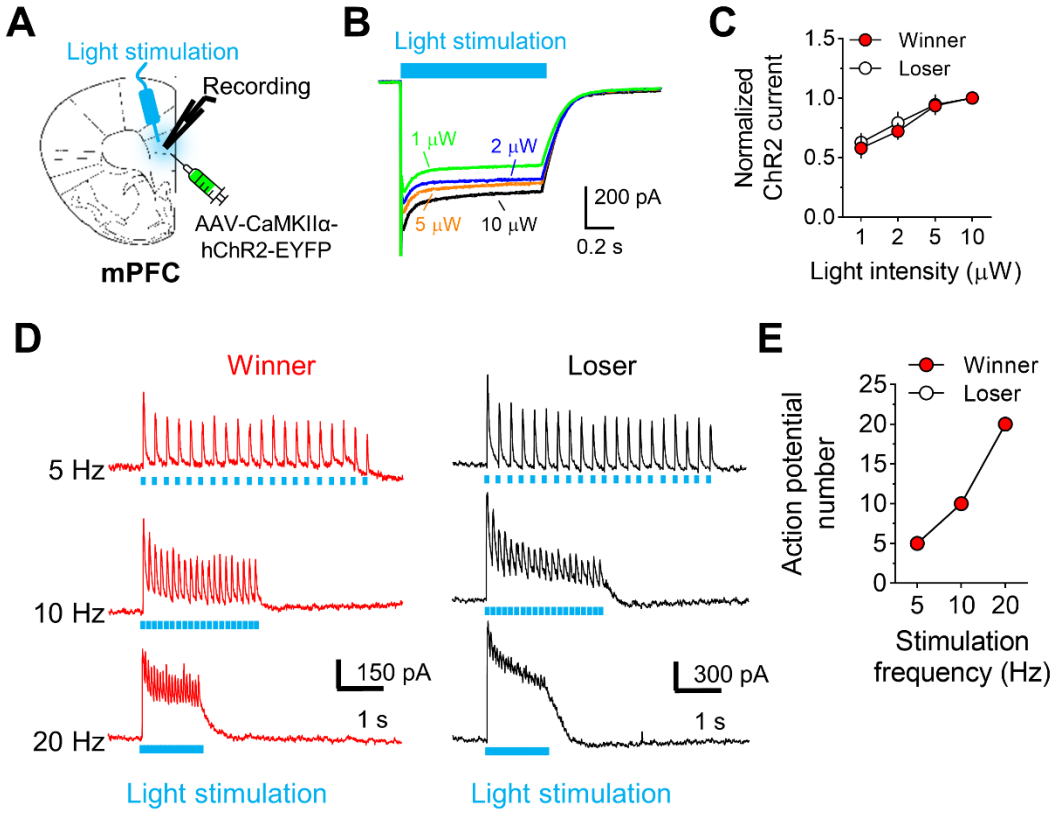

Figure 8. ChR2 currents in the PL neurons from the winner and loser mice.
(A) Schematic showing the light fiber placement and EPSC recording sites in the mPFC.
(B) The representative blue light intensity-dependent photocurrents.
(C) The normalized light intensity-dependent photocurrents in the neurons from winner (red) and loser (black) mice. Winner, n= 12 neurons/ 7 mice; Loser n= 16 neurons/ 7 mice.
(D) The representative traces of action potentials induced by blue lights.
(E) The summarized numbers of action potentials and the frequency of light stimulations. Winner, n= 7 neurons/ 4 mice; Loser n= 7 neurons/ 4 mice.

Data are shown as mean ± SEM. Two-way ANOVA. No significant difference was observed between the winner and loser groups.